The Astrophysical Journal, 685:1114–1128, 2008 October 1

A *SWIFT* GAZE INTO THE 2006 MARCH 29 BURST FOREST OF SGR 1900+14

G. L. Israel,[1] P. Romano,[2,3,4] V. Mangano,[4] S. Dall'Osso,[1,5] G. Chincarini,[2,3] L. Stella,[1] S. Campana,[2] T. Belloni,[2] G. Tagliaferri,[2] A. J. Blustin,[6] T. Sakamoto,[7] K. Hurley,[8] S. Zane,[6] A. Moretti,[2] D. Palmer,[9] C. Guidorzi,[2,3] D. N. Burrows,[10] N. Gehrels,[7] and H. A. Krimm[7,11]

Received 2007 December 21; accepted 2008 May 23

ABSTRACT

In 2006 March the soft gamma-ray repeater SGR 1900+14 resumed its bursting activity after ~2 yr of quiescence. The *Swift* mission observed the source several times. We report on the intense burst "forest" recorded on March 29, which lasted for ~30 s, when *Swift* was pointing at the source with the narrow field of view instruments. More than 40 bursts were detected by BAT and XRT, 7 of which were rare intermediate flares (IFs). The BAT data were used to carry out time-resolved spectroscopy in the 14–100 keV range down to 8 ms timescales. BAT and XRT simultaneous data were used to characterize the broadband energy spectra of IFs and verify the results obtained from the BAT-only spectral fits. This unique data set allowed us to test the magnetar model predictions, such as the magnetically trapped fireball and twisted magnetosphere, over an unprecedented range of fluxes and with large statistics. We confirmed that a two-blackbody component adequately fits the time-resolved and integrated spectra of IFs. However, Comptonization models give comparably good reduced χ^2. Moreover, we found a change of behavior, around $\sim 10^{41}$ erg s^{-1}, above which the softer blackbody shows a sort of saturation, while the harder one still grows to a few times 10^{41} erg s^{-1}, and a rather sharp correlation between temperature and radii of the blackbodies ($R^2 \propto kT^{-3}$), which holds for the most luminous parts of the flares ($\sim L_{\rm tot} \geq 10^{41}$ erg s^{-1}). Within the magnetar model, the majority of these findings are accounted for in terms of thermalized emission from the E-mode and O-mode photospheres. Interestingly, the maximum observed luminosity coming from a region of ~15 km matches the magnetic Eddington luminosity at the same radius, for a surface dipole field of $\sim 8 \times 10^{14}$ G (virtually equal to that deduced from the spin-down of SGR 1900+14).

Subject headings: pulsars: individual (SGR 1900+14) — stars: flare — stars: neutron — X-rays: bursts

Online material: color figures

1. INTRODUCTION

Soft gamma-ray repeaters (SGRs) are a small class of high-energy transient astrophysical sources characterized by their emission of short (~100 ms), bright (10^{39}–10^{42} erg s^{-1}) bursts of soft gamma rays. SGRs have been associated with persistent X-ray counterparts with 1–10 keV luminosity of $\sim 10^{34}$–10^{35} erg s^{-1} and energy spectra that are generally well fit with a power-law model ($\Gamma \sim 2$). A blackbody (BB) component with $kT \sim 0.5$ keV has been found in SGR 1900+14 and SGR 1806−20 (Woods et al. 1999, 2004; Mereghetti et al. 2005). In contrast to the common short bursts, three SGRs have emitted one very powerful long-duration burst. These "giant flares" are distinguished by their extreme energies (10^{44}–$10^{46.5}$ erg s^{-1}), their hard spectra at the onset, and the presence of coherent 5–7 s pulsations at the spin period of the neutron star (NS) during the decaying tail lasting several minutes.

Both SGR 1806−20 and SGR 1900+14 were found to spin down secularly at a rate of $\sim 10^{-11}$ to 10^{-10} s^{-1} (Kouveliotou et al. 1998, 1999). Combining SGR periods and their first derivatives, and assuming that the $B_{\rm dip} \sim 3.2 \times 10^{19} (P\dot{P})^{1/2}$ G relationship generally applied to radio pulsars holds for SGRs as well, magnetic field strengths of 10^{14}–10^{15} G are inferred. The latter values provide strong evidence that SGRs are highly magnetized NSs, i.e., "magnetars" (Duncan & Thompson 1992). In the magnetar model, the magnetic field is the dominant source of free energy (orders of magnitudes higher than the rotational energy of the star), powering the persistent emission through low-level seismic activity and heating of the stellar interior (Thompson & Duncan 1996). When magnetic stresses build up sufficiently to crack a patch of the NS crust, the resulting "crustquake" ejects hot plasma particles into the magnetosphere, which results in an SGR burst (Thompson & Duncan 1995, hereafter TD95). Alternatively, the short SGR bursts may arise from magnetic reconnection events in the stellar magnetosphere (Lyubarsky 2002). Giant flares likely result from a sudden reconfiguration of the star's magnetic field that produces large fractures in the crust and propagates outward through Alfvén waves of enormous power. The ~0.2 s initial spike of giant flares marks the ejection of the largest part of the total event energy (up to $\sim 10^{47}$ erg), as well as the onset of a relatively large surface fracture (Schwartz et al. 2005). The detection of decahertz, hectohertz, and kilohertz QPOs in the decaying phases (tails) of giant flares has been interpreted in terms of global seismic oscillations following the fracture formation (Israel et al. 2005;

[1] INAF–Osservatorio Astronomico di Roma, Via Frascati 33, I-00040 Monteporzio Catone (Roma), Italy; gianluca@mporzio.astro.it, stella@mporzio.astro.it.
[2] INAF–Osservatorio Astronomico di Brera, Via Bianchi 46, I-23807 Merate, Italy.
[3] Università degli Studi di Milano, Bicocca, Piazza delle Scienze 3, I-20126 Milano, Italy.
[4] INAF–Istituto di Astrofisica Spaziale e Fisica Cosmica Sezione di Palermo, Via Ugo La Malfa 153, I-90146 Palermo, Italy.
[5] Dipartmento di Fisica "Enrico Fermi," Universitá di Pisa, Largo Bruno Pontecorvo 3, I-56127 Pisa, Italy.
[6] Mullard Space Science Laboratory, University College London, Holmbury St. Mary, Dorking, Surrey RH5 6NT, UK.
[7] NASA/Goddard Space Flight Center, Greenbelt, MD 20771.
[8] Space Sciences Laboratory, University of California at Berkeley, 7 Gauss Way, Berkeley, CA 94720-7450.
[9] Los Alamos National Laboratory, Los Alamos, NM 87545.
[10] Department of Astronomy and Astrophysics, Pennsylvania State University, University Park, PA 16802.
[11] Universities Space Research Association, 10211 Wincopin Circle, Suite 500, Columbia, MD 21044.

Strohmayer & Watts 2005). The super-Eddington fluxes observed in the tails of these events are thought to be possible because of the suppression of the electron scattering cross sections in the presence of very strong magnetic fields (Paczyński 1992).

Four confirmed SGRs are known so far, three of which are in our Galaxy and one of which is in the Large Magellanic Cloud. The Galactic SGRs are located very close to the plane of the Galaxy, indicating that SGRs belong to a young stellar population. Furthermore, two of these SGRs are likely associated with clusters of very massive stars (Fuchs et al. 1999; Vrba et al. 2000; Eikenberry et al. 2001).

Burst activity in SGRs and, in particular, in SGR 1900+14 occurs sporadically and is quite diverse in behavior. Burst active phases of SGRs vary both in total energy released and in duration, tending to be concentrated into relatively narrow intervals (weeks or months) separated by relatively long periods (years) of quiescence. Following its discovery in 1979, when bursts were detected three times in 3 days, SGR 1900+14 remained in quiescence until 1992, when a handful of bursts were again detected within a few days (Mazets & Golenetskii 1981; Kouveliotou et al. 1993). In 1998 the source entered an unprecedented level of activity during which more than 1000 bursts were recorded within 9 months, and which culminated in the ~400 s long and rather intense 1998 August 27 giant flare event ($\sim 4 \times 10^{44}$ erg s^{-1}). Burst activity was detected until 1999. Particularly interesting are two events detected in 1998 May and September, during which "bunching" of short and long bursts was detected (Hurley et al. 1999; Mazets et al. 1999). Finally, after almost 2 yr of inactivity, on 2001 April 18 an intense and long (~40 s) burst was detected from SGR 1900+14 (Guidorzi et al. 2004). The energy released by this flare (few $\times 10^{42}$ erg) was less than that of the giant flare, although larger than that of the most common short SGR bursts. Consequently, the flare was dubbed an "intermediate flare" (IF; Kouveliotou et al. 2001). Indeed, looking back at the burst history of SGR 1900+14, it was realized that a handful of similar events, characterized by a longer duration (a few seconds to a few tens of seconds) and a higher fluence than those characterizing short bursts, were present. These bursts were then grouped into the class of IFs, likely forming a continuum in terms of duration and fluence (Olive et al. 2004).

A number of broadband spectroscopic studies of short flares and IFs were carried out in the past by different missions. These found that above 15–20 keV, spectra are usually well fitted by an optically thin thermal bremsstrahlung (OTTB) with characteristic temperatures ranging from 20 to 40 keV (Aptekar et al. 2001). Laros et al. (1986) and Fenimore et al. (1994) studied the cumulative spectral properties of 100 bursts from SGR 1806−20 in the 5–200 keV energy range, finding that the number of photons in the spectrum of the detected bursts was remarkably stable in spite of the large intensity spread (a factor of 50) and that the low-energy (below 15 keV) data were inconsistent with the back-extrapolation of an OTTB model that provided a good fit to the high-energy portion of the spectrum. Qualitatively similar spectral properties were measured during a bright IF from SGR 1900+14 using *HETE-2* (Olive et al. 2004) data, which also showed that the OTTB model largely overestimated the flux at low energies (<15 keV). The broadband spectrum (7–100 keV) was best fitted by the sum of two BB laws. Similar conclusions were reported by Strohmayer & Ibrahim (2000) confirming the OTTB limits below 15 keV by using data from the *Rossi X-Ray Timing Explorer*.

Feroci et al. (2004) analyzed the 1.5–100 keV *BeppoSAX* spectral properties of 10 short bursts from SGR 1900+14, further confirming that the widely used OTTB model provides acceptable spectral fits for energies higher than 15 keV but severely overestimates the flux at lower energies. A better fit was obtained by means of an alternative spectral model such as two BBs or a cutoff power law. Most of these studies were hampered by one or more of the following limitations: relatively poor statistics, narrow energy bandpass, poor time resolution, off-axis data, and low sensitivity of wide field of view instruments.

Cumulative analysis of 50 bursts detected by *HETE-2* from SGR 1900+14 showed the presence of a time lag of about 2.2 ± 0.4 ms between the 30–100 and 2–10 keV radiation bands, implying a rapid spectral softening and energy reinjection mechanism (Nakagawa et al. 2007). Alternatively, the softer spectral component could be reprocessed radiation from the harder emission which might be generated near the NS surface. More generally, the observed time lag favors spectral models with (at least) two components. In any case the temperature of the two-BB model does not seem to depend on either the burst intensity or the morphology.

It has been assessed that burst activity in the SGRs can have a persistent effect on the underlying X-ray source (Woods & Thompson 2006 and references therein). During the 1998 burst activity phase of SGR 1900+14, the X-ray counterpart became brighter, its energy spectrum was altered, and the pulse shape changed dramatically. Similar behavior was also recorded from SGR 1806−20 when it resumed its burst activity phase in 2004, culminating with the 2004 December 27 giant flare, and later during the 2005–2006 decaying phase (Woods et al. 2007). It has also been proposed that the bursting activity phases are related to the magnetosphere. The correlation between the persistent X-ray flux and the spectral hardness observed in several magnetar candidates on timescales of years could be accounted for if the evolution were regulated by varying the "twist" of the magnetosphere, as in the case of 1RXS J170849−400910 (Rea et al. 2005a; Israel et al. 2007b) and SGR 1806−20 (Rea et al. 2005b; Woods et al. 2007). As discussed by Thompson et al. (2002), magnetars may differ from standard radio pulsars because their magnetic fields are globally twisted inside the star up to a strength of about 10 times the external dipole and, occasionally, some of their helicity propagates across the NS surface through crustquakes, leading to an impulsive twist of the external field as well. Such an evolving magnetic field is responsible for the different forms of activity and for the glitches. The basic idea of the twist scenario is that when a static twist is formed, currents flow into the magnetosphere. As the twist angle $\Delta\phi_{\rm NS}$ grows, electrons provide increasing optical depth to resonant cyclotron scattering, leading to the buildup of a flatter photon power-law component. At the same time, returning currents produce extra heating of the star surface and increased X-ray flux. The few long-term X-ray monitoring observations of magnetars collected until now are consistent with a scenario in which the twist angle steadily increased before the glitch epochs, culminating with glitches, sometimes bursts, and a period of increased timing noise, and then decreased, leading to a smaller flux and a softer spectrum.

In this paper, we report the results obtained from our analysis of the data collected by the *Swift* Burst Alert Telescope (BAT; Barthelmy et al. 2005) and X-Ray Telescope (XRT; Burrows et al. 2005), which monitored SGR 1900+14 during a burst active phase in 2006 March (Palmer et al. 2006). SGR 1900+14 triggered BAT five times in a few days at the end of 2006 March, and once a couple of months later. In particular, on March 29 (Romano et al. 2006a) an extremely intense emission event [fluence of $\sim(2–3) \times 10^{42}$ erg], lasting ~30 s, of short and relatively energetic bursts was recorded while both BAT and XRT were simultaneously observing the source, thanks to an automatic slew performed in response to a previous trigger. About 40 single bursts

TABLE 1
SGR 1900+14 *Swift* Observation Log for Pointings Carried out during 2006

Sequence	Obs/Mode	Start Time (UT)	End Time (UT)	Exposure (s)
00202746000[a]	BAT/EVENT	2006 Mar 25, 20:16:30	2006 Mar 25, 20:17:13	43
00203045000[b]	BAT/EVENT	2006 Mar 28, 13:50:05	2006 Mar 28, 13:50:48	43
00203109000[c]	BAT/EVENT	2006 Mar 29, 01:27:53	2006 Mar 29, 01:28:36	43
00203127000[d]	BAT/EVENT	2006 Mar 29, 02:52:50	2006 Mar 29, 02:53:42	50
00203974000[e]	BAT/EVENT	2006 Apr 5, 06:43:21	2006 Apr 5, 06:44:04	43
00214277000[f]	BAT/EVENT	2006 Jun 10, 06:49:02	2006 Jun 10, 07:09:04	1202
00030386001	XRT/PC	2006 Mar 25, 22:50:43	2006 Mar 27, 21:47:47	49564
00030386002	XRT/PC	2006 Mar 28, 01:05:28	2006 Mar 28, 23:48:57	11350
00030386003	XRT/WT	2006 Mar 29, 01:01:00	2006 Mar 29, 23:57:00	18592
00030386004	XRT/WT	2006 Mar 30, 01:07:00	2006 Mar 30, 23:59:58	20055
00030386005	XRT/WT	2006 Mar 31, 01:26:23	2006 Mar 31, 23:59:59	15931
00030386006	XRT/WT	2006 Apr 1, 01:13:58	2006 Apr 3, 13:12:31	45951
00030386008	XRT/WT	2006 Apr 7, 11:48:02	2006 Apr 7, 23:20:00	7846
00030386009	XRT/PC	2006 Apr 8, 00:51:04	2006 Apr 10, 23:38:58	29274
00030386010	XRT/PC	2006 Apr 11, 00:48:12	2006 Apr 11, 23:44:55	18250
00030386011	XRT/PC	2006 Apr 12, 00:47:49	2006 Apr 12, 23:43:57	20503
00030386012	XRT/PC	2006 Apr 13, 00:53:42	2006 Apr 13, 18:41:34	10702
00030386013	XRT/PC	2006 Apr 14, 22:22:41	2006 Apr 14, 23:59:56	1602
00214277000	XRT/PC	2006 Jun 10, 06:54:59	2006 Jun 10, 08:56:03	4071

[a] First BAT trigger: 2006 March 25, 20:16:40.28 UT.
[b] Second BAT trigger: 2006 March 28, 13:50:15.00 UT.
[c] Third BAT trigger: 2006 March 29, 01:28:03.99 UT.
[d] Fourth BAT trigger: 2006 March 29, 02:53:09.46 UT.
[e] Fifth BAT trigger: 2006 April 5, 06:43:31.36 UT.
[f] Sixth BAT trigger: 2006 June 10, 06:53:00.80 UT.

were detected during this "forest," or "storm"; a handful were long enough ($\geq$500 ms) to be considered IFs. The unprecedented BAT and XRT statistics allowed us to perform both average and time-resolved spectral analysis in the 1–100 keV band, the first ever on a large sample of IFs on millisecond timescales. We also studied the persistent emission of SGR 1900+14 preceding and following the forest in a search for transient and permanent spectral variations on timescales of days and weeks, timescales which have been rarely studied. The timing properties of the event are discussed in an accompanying paper (D. Palmer et al. 2008, in preparation).

2. OBSERVATIONS AND DATA REDUCTION

Table 1 reports the log of the *Swift* observations of SGR 1900+14 that were used for this work. The BAT data of the bursts were accumulated in event mode, with full temporal and spectral resolution, and archived in sequences labeled by the BAT trigger number (the first six sequences in Table 1). The sequence corresponding to the March 29 forest is 00203127000.

The XRT data of pointed observations were archived in the following 13 sequences of Table 1, which span from 2006 March 25 to June 10. Note that the XRT data of the forest are stored in sequence 0030386003.

The BAT data were analyzed using the standard BAT analysis software distributed within FTOOLS version 6.0.5. The arrival times of events were converted to arrival times in the reference frame of the solar system barycenter (SSB) using the `barycorr` task. Mask-weighted (i.e., background-subtracted) light curves were created from event data in the 15–25, 25–40, 40–100, and 15–100 keV energy ranges at 1 and 4 ms time resolution (see Fig. 1 and the bottom four panels of Fig. 2 for the light curves of the March 29 forest). Response matrices for BAT spectra were generated with the task `batdrmgen` using the latest spectral redistribution matrices. For our spectral fitting (XSPEC ver. 12.2.1) we considered the 14–100 keV energy range and applied an energy-dependent systematic error vector.[12] The time resolution of BAT is 100 μs, so pileup is never an issue under normal circumstances (see Barthelmy et al. 2005). No dead-time effects have been found for these observations (BAT team 2006, private communication).

The XRT data were first processed by the *Swift* Data Center at NASA/GSFC into Level 1 products (calibrated and quality-flagged event lists). Then they were further processed with HEASOFT (ver. 6.0.5) to produce the final cleaned event lists. In particular, we ran the task `xrtpipeline` (ver. 0.10.3), applying standard filtering and screening criteria; i.e., we cut out temporal intervals during which the CCD temperature was higher than -47°C, and we removed hot and flickering pixels which were present because the CCD operated at a temperature higher than the design temperature of -100°C due to a failure in the active cooling system. An onboard event threshold of $\sim$0.2 keV was also applied to the central pixel, which has been proved to reduce most of the background due to either the bright Earth limb or the CCD dark current (which depends on the CCD temperature).

For our analysis we considered windowed-timing (WT) and photon-counting (PC) mode data (see Hill et al. 2004 for a full description of readout modes) and further selected XRT event grades 0–12 and 0–2 for the WT and PC data, respectively (see Burrows et al. 2005). The arrival times of events were converted to arrival times in the reference frame of the SSB.

During sequence 00030386003 (i.e., the forest) the count rate of the outburst was high enough to cause pileup even in the WT mode data. Therefore, to account for this effect, the WT data were extracted in a rectangular 40×20 pixel region with a 4×20 or 6×20 pixel region excluded from its center depending on the peak source intensity, i.e., with a 4×20 pixel exclusion region

[12] See http://heasarc.gsfc.nasa.gov/docs/swift/analysis/bat_digest.html.

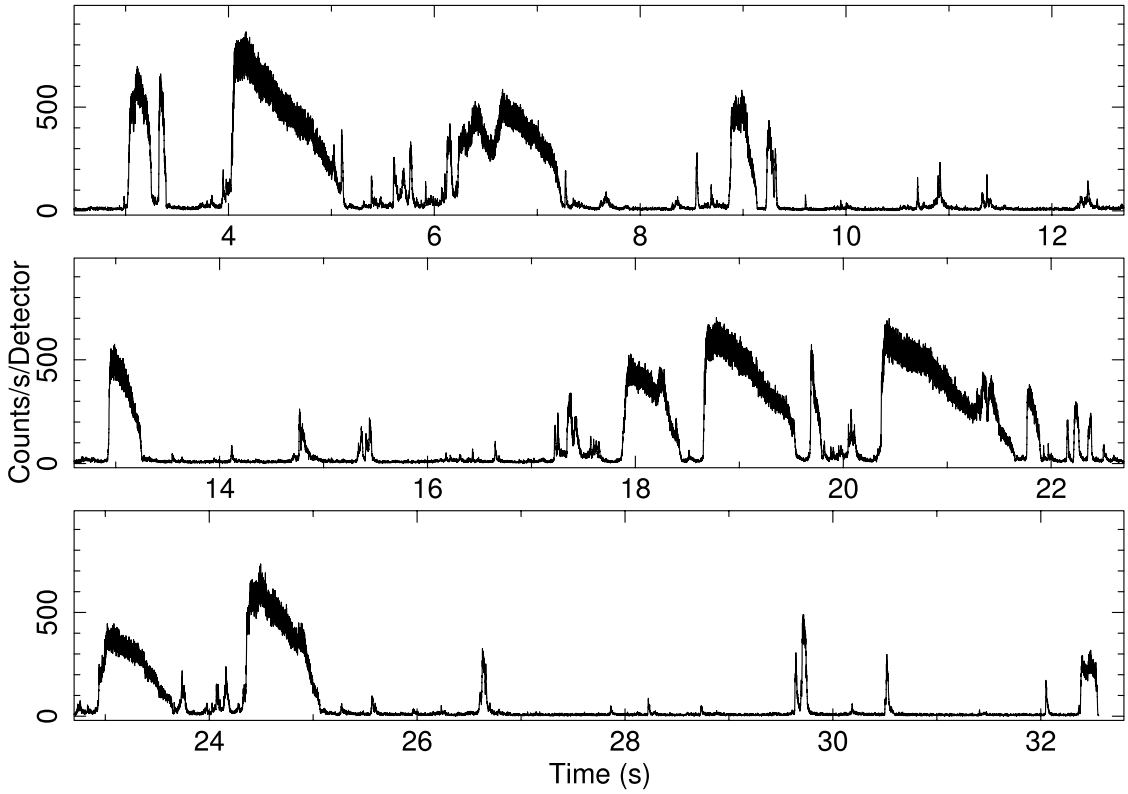

FIG. 1.—The 15–100 keV BAT light curves with a time resolution of 1 ms obtained during the burst forest of 2006 March 29.

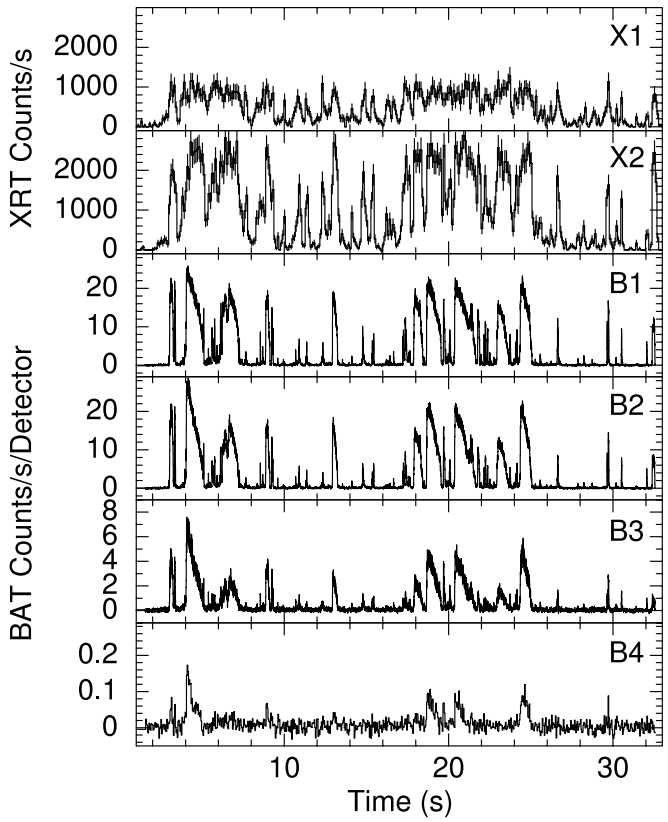

FIG. 2.—BAT and XRT WT light curves obtained simultaneously during the burst forest of 2006 March 29. Different energy ranges are shown: 1–4 and 4–10 keV for the XRT (panels X1 and X2, respectively), and 15–25, 25–40, 40–100, and >100 keV for the BAT (panels B1, B2, B3, and B4, respectively). The XRT light curves were background-subtracted and corrected for vignetting, PSF losses, and pileup effects. It is evident from the comparison of XRT and BAT light curves that, on average, the IFs are harder than the short bursts, although notable exceptions are present.

during the first and third snapshots[13] (where the observed count rate reached $\approx$350 counts s^{-1}) and with a 6×20 pixel exclusion region during the second snapshot (where the observed count rate reached $\approx$1300 counts s^{-1}). The size of the exclusion region was determined following the procedure illustrated in Romano et al. (2006b) and corresponded to 30%–39% (4–6 pixel hole) of the XRT PSF. Ancillary response files were generated with the task `xrtmkarf` within FTOOLS and account for different extraction regions and PSF corrections. We used the latest spectral redistribution matrices in the calibration database maintained by HEASARC.

The PC data show an average count rate of $\sim$0.08 counts s^{-1} throughout the entire monitoring campaign; therefore, no pileup correction was necessary. We extracted the source events in a circle with a radius of 20 pixels ($\sim$47″). To account for the background, we extracted WT events within a rectangular box (40×20 pixels) and PC events within an annular region (radii 85 and 110 pixels) centered on the source and far from background sources.

The energy-resolved light curves during the burst active phase are shown in Figure 2 for both the XRT (panels X1 and X2) and the BAT (panels B1–B4). The XRT light curves were background-subtracted and corrected for vignetting and PSF losses, as well as for pileup.

2.1. *Time-resolved BAT Spectroscopy*

This section refers to the analysis of the BAT data set recorded after the fourth trigger (sequence 00203127000; see Table 1). In consideration of the extremely pronounced variability of the source during the burst active phase, we adopted the following strategy for the time-resolved spectroscopic analysis: we selected a 4000 count threshold for the accumulation of each spectrum. This resulted in a set of 729 BAT mask-weighted (i.e., background-subtracted) spectra extracted from the event data of sequence

[13] A snapshot is a continuous pointing at the target.

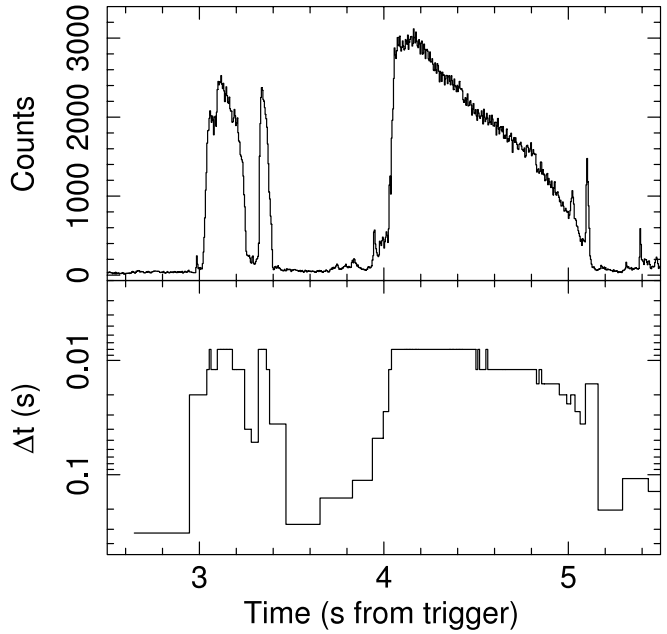

FIG. 3.— Outcome of the selection criterion of relying on a minimum of 4000 photons in each spectrum. For the first 3 s of the 2006 March 29 forest we reported the net counts (*top*) and the integration time (*bottom*).

00203127000. The choice of the threshold is our best trade-off for optimizing the signal-to-noise ratio of the spectra while still closely following the sharpest features of the light curve. Figure 3 shows the results of our spectral accumulation criterion for the first 3 s of the BAT light curve. In particular, the choice of 4000 counts per spectrum is such that (1) the rapid increase of the first IF is well sampled, (2) the first two short bursts (peaking at about 3.10 and 3.35 s) are resolved in time, and (3) 90% of the IF decay is sampled with a time resolution of $\leq$10 ms. All spectral channels with poor statistics (below 20 counts) were removed before fitting. The resulting accumulation time of the BAT spectra ranges from 8 to about 400 ms.

Several different spectral models were adopted in the fit of the whole sample of 729 spectra in an automatic fashion. For each spectrum and model we recorded the values of the best-fit parameters, unabsorbed flux, and reduced χ^2. Then, we averaged the measured χ^2 and inferred their standard deviations. The latter quantities can be considered a qualitative indication of the spectral model fit goodness, on average. The results are given in Table 2, ordered by the increasing number of degrees of freedom in the adopted model.

Similarly to previous studies reported above and in the literature, we tested both single and multicomponent models. Former models include an OTTB (Bremss), given that it was found to well describe the hard X-ray spectra of SGR bursts; a power law with an exponential cutoff (CutoffPL), which may be considered an extension of the simple OTTB; a disk blackbody (DiskBB), which is a generalization of a thermal spectrum also including geometrical parameters; and different versions of a Comptonized spectrum (such as CompST) representative of models involving a thermal spectrum modified by mechanisms which preserve the photon number. Among the double-component models we considered a two-blackbody (BB+BB) model able to well fit the broadband energy spectra of both short and long SGR bursts, an OTTB with a soft BB in order to adjust the OTTB model extrapolation at low energy, and a Comptonization model where soft photons are upscattered in a hot plasma taking into account relativistic effects (CompTT; Titarchuk 1994), which is, as a first approximation, a generalization of both the BB+BB model (in the case of saturated Comptonization) and the CompST model.

TABLE 2
SUMMARY OF THE AVERAGE REDUCED χ^2 AND STANDARD DEVIATION FOR DIFFERENT SINGLE-COMPONENT AND MULTICOMPONENT MODELS

	BAT+XRT[a]		BAT		
SPECTRAL MODEL	$\langle\chi^2_\nu\rangle$	σ	$\langle\chi^2_\nu\rangle$	σ	NO. OF PARAMETERS
Bremss	4.84	1.17	1.71	1.95	2
DiskBB	2.91	0.84	1.17	0.51	2
CompST	2.41	0.16	1.08	0.42	3
CutoffPL	1.36	0.07	1.07	0.23	3
Bremss+BB	1.33	0.25	1.06	0.28	4
CompTT	0.88	0.07	0.99	0.17	4
BB+BB	0.88	0.08	1.01	0.16	4
Bremss[b]	...	...	0.91	0.11	2

NOTE.— Obtained for the 729 time-resolved BAT spectra and the 8 BAT+XRT spectra of the most intense bursts.
[a] We used a free scaling factor between XRT and BAT of the order of 10%.
[b] Fit carried out in the 15–50 keV range.

The procedure of increasing new spectral components (therefore increasing the number of free parameters) was stopped when the *F*-test probability for the inclusion of an additional component became less than 3 σ. It is evident from Table 2 that, for BAT spectra, small (close to unity) reduced χ^2 are obtained for one or two component models with free parameters $\geq$3. Moreover, for BAT+XRT joined spectra, small reduced χ^2 are obtained only for two-component models with four free parameters. The inclusion of a third component (five or six free parameters) is not statistically significant.

The CompTT and BB+BB models are by far those that give the best reduced χ^2 (average of 0.99 and 1.01). Moreover, as already reported by several authors, while the OTTB model fits the spectra well on relatively narrow energy ranges (reduced $\chi^2 \approx 0.9$ in the 15–50 keV range), it fails to produce an acceptable fit once a broader energy interval is considered (reduced $\chi^2 \approx 1.7$ in the 14–100 keV energy range). A better description is obtained by adding a BB component to the OTTB spectrum (reduced $\chi^2 \approx 1.07$). This additional BB component turns out to have a characteristic temperature similar to that of the softer BB component in the BB+BB model.

The average temperatures and sizes of the BB components in the BB+BB model during the IFs are $\langle kT_{\rm soft}\rangle = 4.8 \pm 0.3$ keV with $\langle R_{\rm soft}\rangle = 30 \pm 2$ km and $\langle kT_{\rm hard}\rangle = 9.0 \pm 0.3$ keV with $\langle R_{\rm hard}\rangle = 5.7 \pm 0.5$ km, which are in good agreement with previous results based on an IF (Olive et al. 2004) and a large sample of short bursts (Nakagawa et al. 2007). However, with respect to the latter cases, the present *Swift* data represent the best opportunity (so far) to study the above reported spectral parameters as a function of time with good statistics coupled to fine timing resolution. Figure 4 shows, as an example, the results of the automatic spectral fitting in the case of the BB+BB model for the first 3 s of the high time resolution BAT data, while in Figures 5 and 6 we use the inferred values for the entire 30 s duration and try to characterize the main properties of the adopted model.

2.2. *Time-resolved BAT+XRT Spectroscopy*

A joint fit of the BAT and simultaneous XRT WT data of the bursting phase associated with the fourth trigger was performed with a second set of eight BAT and XRT WT spectra (sequences 00203127000 and 00030386003). The eight time intervals during which these spectra were accumulated correspond to the occurrence

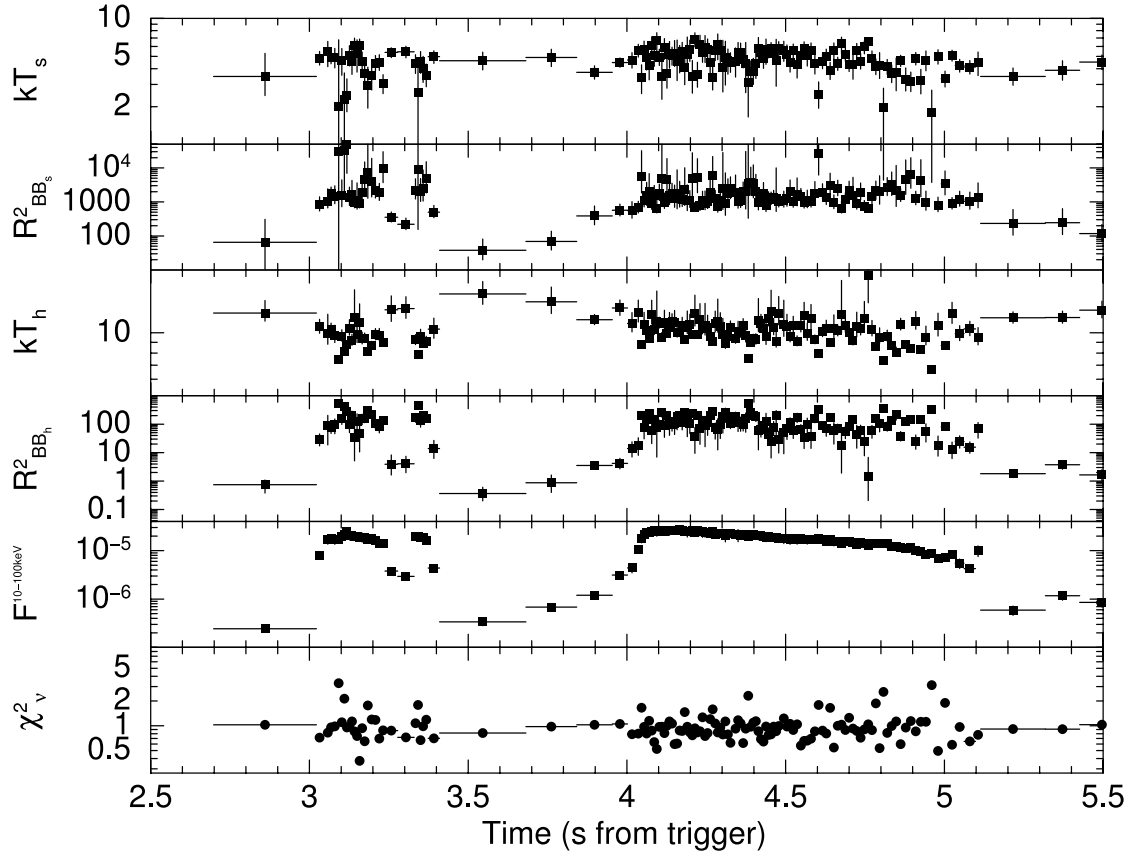

FIG. 4.— Time-resolved results from the spectral fits obtained in the case of the BB+BB model for the first 3 s of the BAT light curve. The soft BB temperature and radius and the hard BB temperature and radius are reported together with the observed flux in the 10–100 keV band and the reduced χ^2 (*top to bottom*).

of the seven IFs plus a canonical short burst (as a comparison). We report the main spectral parameters in Tables 2 and 3.

The results of the XRT+BAT fits (see Table 2) confirm those obtained with the BAT in the previous section: the CompTT and the BB+BB models give the best reduced χ^2 ($\approx$0.9), and the OTTB (Bremss; Table 2 and hereafter) give the worst. However, when a BB component is added to the latter component, a better solution is obtained, with a number of dof equal to that of the CompTT and BB+BB models, although the reduced χ^2 ($\approx$1.3; Table 2) remains too high to be acceptable. More generally, the addition of a BB component to the other poorly fitted models, such as the CompST and CutoffPL, results in a smaller reduced χ^2, although a not yet acceptable one with a larger number of free parameters (five). In all cases the characteristic temperature of the soft thermal component is similar to that of the soft BB in the BB+BB model. These findings, together with similar results obtained by the analysis of broadband spectra of SGR bursts from other missions, in slightly different (but overlapping) energy intervals, and by using different procedures/algorithms, make us confident that the *Swift* fitting results are reliable.

We note that adopting a different abundance than solar values for the absorption multiplicative component (Anders & Grevesse 1989; Lodders 2003) does not significantly modify the spectral parameters for the joint XRT+BAT spectral fit.

2.3. *XRT Monitoring of the Persistent Emission*

The approximately 2 month time span covered by the *Swift* monitoring observations was also used to study the timing and spectral properties of the persistent emission. Only the PC data were used for spectral analysis in order to rely on a better signal-to-noise ratio. WT data were also accumulated and used for timing analysis, after removing the bursts, in order to rely on a higher time resolution. The corresponding *Swift* data sequences used to carry out the spectral analysis are 00030386001 ($\approx$50 ks effective exposure time), 00030386002 ($\approx$11 ks), 00030386009 ($\approx$29 ks), and 00030386010–6013 ($\approx$51 ks). In order to minimize the possible burst contamination in PC mode, spectra were accumulated after having excluded an $\sim$10 s time interval just before and after each good time interval corresponding to automatic switches between PC and WT modes. In fact, these switches are likely due to high count rate events from cosmic rays and/or from genuine bursts from SGR 1900+14. A comparison between the filtered and unfiltered spectra did not result in the detection of significant differences, making us confident that burst contamination, if any, is negligible. As in the previous cases, the data were rebinned with a minimum of 20 counts per energy bin to allow χ^2 fitting within XSPEC (ver. 12.2.1). We further removed those energy channels with poor statistics after background subtraction.

We assumed an absorbed power law plus BB model as inferred with deeper *XMM-Newton* observations (Mereghetti et al. 2006). We left the absorption free to vary but forced it to be the same in different spectra and obtained $N_{\rm H} = (2.3 \pm 0.1) \times 10^{22}$ cm^{-2}. The results of the fits are reported in Table 4, while fitted spectra are shown in Figure 7 together with their residuals expressed in units of σ. There is marginal evidence of parameter variability as a function of observed flux; the spectrum becomes harder for larger flux levels. In order to properly quantify such spectral variability and its flux dependence, we carried out a bidimensional fit (contour plot) of the main spectral parameters, which also has the advantage of better taking into account the possible correlations among them. The results of these additional fits are shown in Figures 8 and 9. The ellipsoidal shape of the 1, 2, and 3 σ confidence

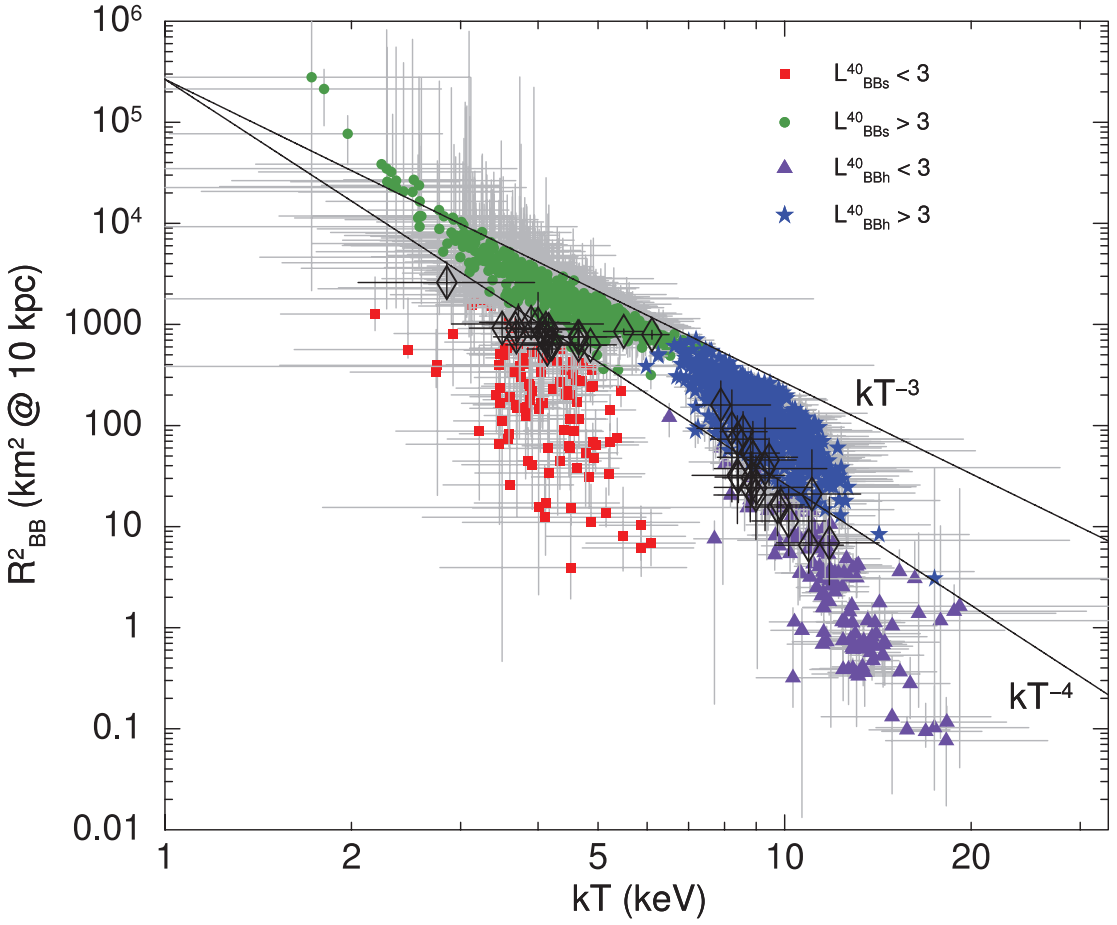

FIG. 5.—Square of the radii of the two BBs as a function of their temperatures for the whole ~30 s BAT data set. Red squares and green circles mark the BB_s component for luminosities below and above 3×10^{40} erg s^{-1}, respectively. Violet triangles and blue stars indicate the same quantities for the BB_h component. Black diamonds mark the Olive et al. (2004) measurements obtained for the 2001 IF. We also plot two representative power laws for $R^2 = kT^{\alpha}$, with α equal to −3 and −4 (the latter corresponding to the expected relation for a pure BB).

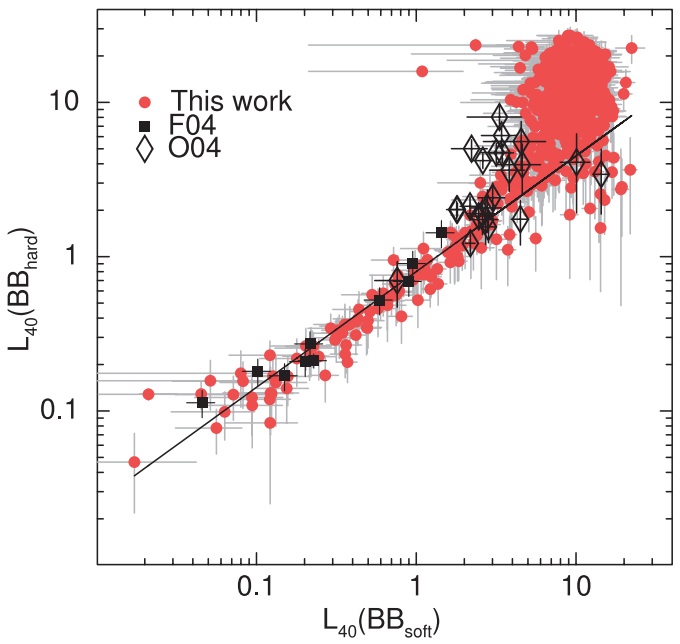

FIG. 6.—Time-resolved bolometric luminosity of BB_{soft} vs. that of BB_{hard} (in units of 10^{40}). The solid line marks the power-law relation $L^{40}_{soft} = (L^{40}_{hard})^{\alpha}$ with $\alpha = 0.70 \pm 0.03$ (1 σ c.l.) obtained by fitting points in the $0.01-3\ L^{40}_{soft}$ range. Squares represent the measurements by Feroci et al. (2004) for short bursts.

regions (the innermost region corresponding to 1 σ) clearly indicates that the parameters (and, more generally, the BB and PL components) correlate with each other. In addition, the two-parameter fits confirm the spectral evolution (c.l. >3 σ) of the persistent spectrum of SGR 1900+14 as a function of flux; the source displayed harder spectra just before (March 28) and after (April 8) the burst forest event (March 29) and returned to the preevent level in mid-April. These results are similar to those observed in other magnetar candidates, such as SGR 1806−20 among SGRs and 1RXS J170849−400910 among anomalous X-ray pulsars (AXPs), the main difference being the timescales on which these spectral variations occurred: years for the latter two sources and days/weeks for SGR 1900+14. In the previous cases this trend has been modeled in terms of "twisting" of the magnetosphere (Thompson et al. 2002).

The WT and PC XRT data were also used to look for the ~5.2 s pulsations of SGR 1900+14. Given the limited XRT statistics in the persistent component and the relatively small pulsed fraction of the pulses (~15%–20% level; semiamplitude of modulation divided by the mean source count rate), we used the period value, $P = 5.19987 \pm 0.00007$ s, inferred from an *XMM-Newton* observation carried out on 2006 April 1 (Mereghetti et al. 2006). We detected the SGR 1900+14 pulsations on 2006 March 29, the same day as the burst forest event, in two time intervals preceding (March 29 from 01:02 to 01:26 UT) and following (from 04:22 to 04:42 UT) the forest by approximately 1 hr (in both cases the signal was detected at about 3 σ c.l.). By merging all the XRT

TABLE 3
XRT WT and BAT Spectral Fit Results of the Seven Identified IFs and One Short Burst for the BB+BB Model

Bin	$N_{\rm H}$ (10^{22} cm^{-2})	kT (keV)	$R_{\rm BBs}$[a] (km)	kT_h (keV)	$R_{\rm BBs}$[a] (km)	$F_{\rm X}^{1-10\ {\rm keV}}$ ($\times10^{-7}$ erg cm^{-2} s^{-1})	$F_{\rm X}^{10-100\ {\rm keV}}$ ($\times10^{-7}$ erg cm^{-2} s^{-1})	$\chi^2_{\rm red}$	dof
IF1	2.0 ± 0.3	6.2 ± 0.3	15.9 ± 4.2	12.0 ± 0.3	3.5 ± 1.2	4.68 ± 0.15	103.1 ± 1.8	0.84	135
IF2	1.9 ± 0.3	5.6 ± 0.3	17.6 ± 4.7	10.4 ± 0.3	3.6 ± 1.5	4.77 ± 0.15	64.4 ± 1.7	1.15	153
SB	1.2 ± 0.3	5.5 ± 0.3	13.4 ± 4.0	12.1 ± 0.4	2.2 ± 0.8	2.71 ± 0.13	29.1 ± 0.9	0.77	105
IF3	2.1 ± 0.6	5.4 ± 0.3	17.1 ± 5.4	10.2 ± 0.4	3.6 ± 1.6	4.29 ± 0.24	74.5 ± 1.9	0.97	100
IF4	2.1 ± 0.5	6.1 ± 0.3	17.4 ± 4.9	11.7 ± 0.3	3.7 ± 1.4	5.49 ± 0.23	127.8 ± 3.0	0.88	115
IF5	2.8 ± 0.4	6.1 ± 0.3	17.1 ± 4.6	11.0 ± 0.3	4.1 ± 1.6	5.19 ± 0.17	89.8 ± 2.4	1.07	146
IF6	2.3 ± 0.4	5.1 ± 0.3	19.0 ± 5.9	9.8 ± 0.3	3.8 ± 1.6	4.70 ± 0.18	53.5 ± 1.9	0.73	117
IF7	2.7 ± 0.5	5.7 ± 0.3	17.1 ± 5.1	11.6 ± 0.3	3.6 ± 1.2	4.71 ± 0.20	85.1 ± 2.8	0.77	116

Note.—Fluxes are not corrected for $N_{\rm H}$.
[a] Assuming a distance to the source of 10 kpc.

observations carried out in March/April (from March 30 01:07 to April 7 23:20) and by using $\dot{P} = (9.2 \pm 0.4) \times 10^{-11}$ s^{-1} reported by Mereghetti et al. (2006), the pulsations could be detected at a high significance level. Figure 10 summarizes the results of the timing analysis. Both the pulse fractions and the shapes inferred from the first data set are different from those obtained from the second and third data sets and, more generally, from what has been observed on average since the discovery of this source. At the same time, the pulse shapes of the second and third data sets are significantly different. The value and shape of the latest data set are virtually equal (to within the uncertainties) to those obtained by Mereghetti et al. (2006) about 3 days after the BAT event.

2.4. *UVOT Observations and Data Reduction*

The *Swift* UV/Optical Telescope (UVOT; Roming et al. 2005) is a 30 cm modified Ritchey-Chrétien telescope coaligned with the XRT. It features a PC microchannel plate-intensified CCD detector optimized for UV and optical light over the 170–600 nm range; its six broadband color filters sample this range.

The UVOT was taking data in the *V* filter (central wavelength 5460 Å) during the March 29 outbursts of SGR 1900+14. No optical counterpart is detected in the resulting image, accumulated between 02:39:57 and 03:06:00 UT with a total exposure time of 1539 s. In the following we derive an upper limit to the optical emission during the burst forest. Counts were extracted from a 2″ radius aperture at the position of the source in the XRT; the size of the aperture was chosen so as to minimize contamination by a $V \sim 18.6$ mag star (USNO No. 0975-14353360) which is only 3″ from the XRT position. The counts were aperture-corrected up to 6″ and used to calculate a 3 σ *V*-band magnitude upper limit for any counterpart of 20.7 mag. Adopting the Akerlof et al. (2000) estimate for A_V of $\sim$10 mag for Galactic reddening in the direction of SGR 1900+14, we estimated a dereddened upper limit of 10.7 mag.

For each UVOT image coincident with an outburst, counts were extracted from 4″ radius apertures at the position of the source in the XRT. The counts were aperture-corrected up to 6″ (optical filters) or 12″ (UV filters; the different apertures are due to the broader PSF in the UV) and used to calculate 3 σ magnitude upper limits for any counterpart. Using the Akerlof et al. (2000) estimate of $A_V \sim 10$ mag for the Galactic reddening in the direction of SGR 1900+14, we corrected the upper limits for Galactic extinction assuming $E(B - V) = 3.125$. The resulting values are listed in Table 5.

3. DISCUSSION

Exploiting its rapid follow-up pointing capability, *Swift* recorded a rather intense and rare series of short bursts and IFs (the densest part of which lasted for $\sim$30 s) from SGR 1900+14 during 2006 March. This allowed us to carry out, for the first time, a detailed study of the average and time-resolved spectral properties of this source during such events. Moreover, the continuous monitoring of SGR 1900+14 on longer timescales afforded a study of the changes of the spectral and timing properties of the persistent emission.

3.1. *Burst Emission*

We used several different spectral models comprising one or two components to fit both the time-resolved BAT spectra and the time-averaged (over a whole single burst or IF) BAT+XRT spectra. Interestingly, only two (CompTT and BB+BB) out of the five models considered (CompST, CutoffPL, Bremss+BB, CompTT, and BB+BB) which fit the BAT spectra well are also able to model the BAT+XRT spectra (see Tables 2 and 3). An OTTB (Bremss)

TABLE 4
XRT PC Spectral Fit Results of the Persistent Emission of SGR 1900+14

Interval (MJD)	kT (keV)	$R_{\rm BBs}$[a] (km)	Γ	$F_{\rm X}^{1-10\ {\rm keV}}$ ($\times10^{-12}$ erg cm^{-2} s^{-1})	$\chi^2_{\rm red}$	dof
53,819.9519–53,821.9082	0.39 ± 0.02	3.4 ± 0.5	2.4 ± 0.1	4.6 ± 0.8	1.13	125
53,822.0455–53,822.9923	0.51 ± 0.06	2.9 ± 0.6	1.9 ± 0.3	6.3 ± 1.7	0.91	39
53,833.0355–53,835.9854	0.48 ± 0.03	3.3 ± 0.4	2.1 ± 0.2	5.0 ± 1.4	0.96	86
53,836.0335–53,840.0000	0.38 ± 0.02	4.3 ± 0.8	2.3 ± 0.1	5.0 ± 0.7	0.94	137

Notes.—During the four time intervals reported in the text and by assuming the BB+PL model. Fluxes are not corrected for the $N_{\rm H}$ value (which is left to vary but constant among spectra).
[a] Assuming a distance to the source of 10 kpc and an absorption hydrogen column of $(2.3 \pm 0.1) \times 10^{22}$ cm^{-2}.

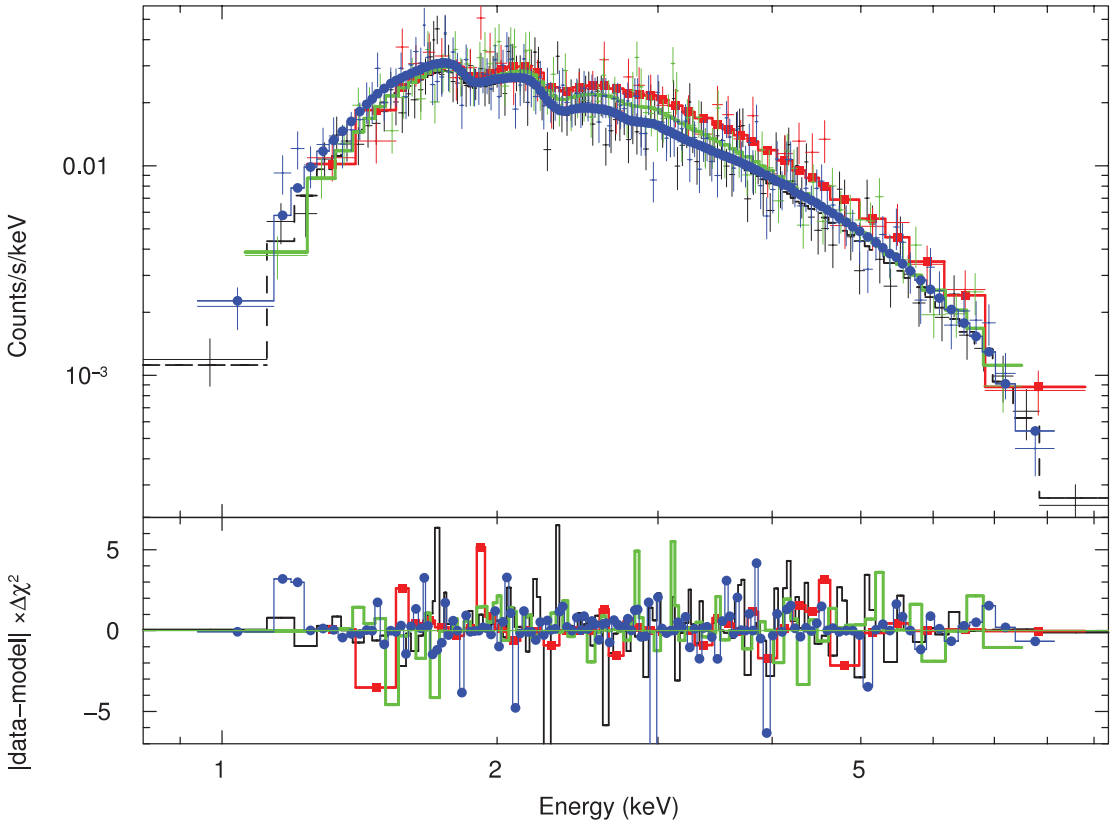

FIG. 7.—The 1–10 keV *Swift* XRT spectra (PC mode only) of the persistent emission of SGR 1900+14, shown with the model (BB+PL) residuals. The corresponding *Swift* data sequences are 00030386001 (*black lines*), 00030386002 (*red lines and squares*), 00030386009 (*green lines*), and 00030386010–6014 (*blue lines and circles*).

does not yield an acceptable reduced χ^2 in either case (BAT and BAT+XRT spectra). This result is consistent with previous spectral analyses carried out on broadband spectra of a few short bursts and a 4 s long IF (see Feroci et al. 2004; Olive et al. 2004). Notably, the Bremss model describes the BAT spectra well only when a reduced energy interval, 15–50 keV, is considered. In the following we discuss in greater detail the results inferred from the BB+BB model (note that the CompTT model shape is virtually identical to that of the BB+BB in the limit of saturated Comptonization). Moreover, in consideration of the difficulties in explaining short bursts and IFs in the accretion scenario (extreme super-Eddington luminosities are, in fact, observed), we discuss here the implications of our results within the magnetar scenario.

With respect to the former studies of the broadband spectrum of similar events, the *Swift* observation of 2006 March 29 has the

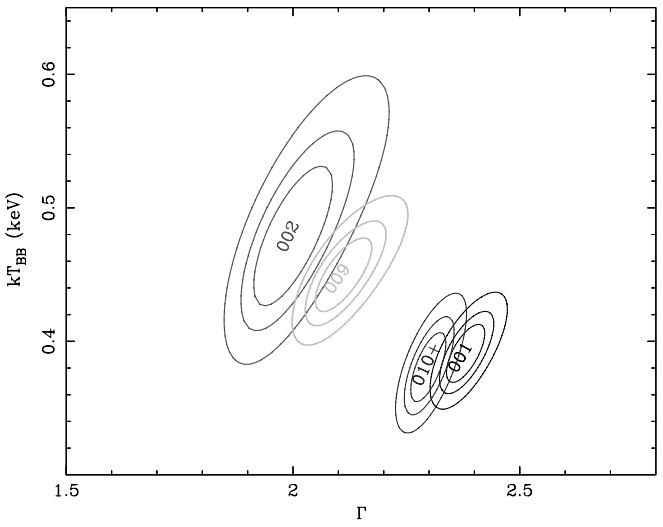

FIG. 8.—The 1, 2, and 3 σ confidence regions obtained for the BB temperature kT and the power-law photon index Γ for each spectrum during persistent emission from SGR 1900+14. Note that the temperature kT is consistent with being constant, while Γ is variable and harder than in quiescence, at the more than 3 σ level. [*See the electronic edition of the Journal for a color version of this figure.*]

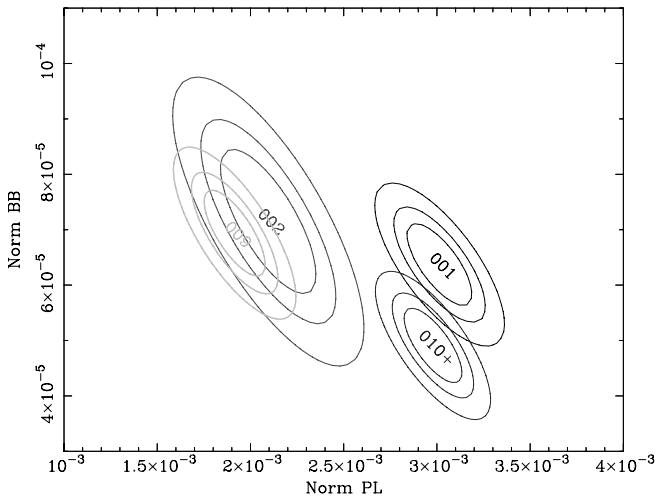

FIG. 9.—The 1, 2, and 3 σ confidence regions obtained for the BB and PL normalizations for each spectrum during persistent emission from SGR 1900+14. Similar to Fig. 8, the BB component appears to be approximately constant, while the PL normalization is variable and higher than in quiescence, at the more than 3 σ level. [*See the electronic edition of the Journal for a color version of this figure.*]

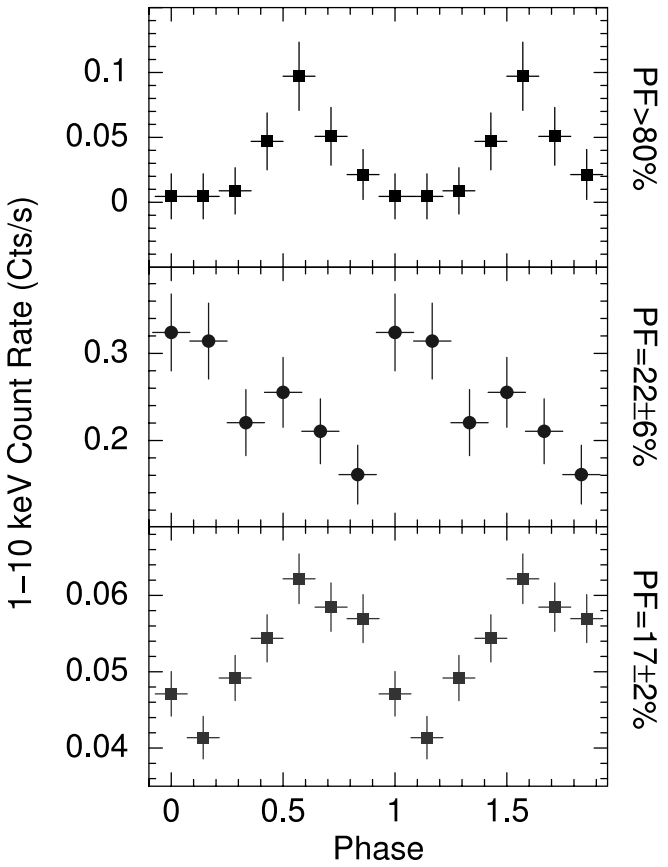

FIG. 10.—The 1–10 keV *Swift* XRT light curves of SGR 1900+14 from approximately 1 hr before and after the BAT event (2006 March 29; *top and middle*) and the first week of 2006 April (*bottom*). In all cases we used $P = 5.19987 \pm 0.00007$ s, as determined from an *XMM-Newton* observation carried out on 2006 April 1 (Mereghetti et al. 2006). For the approximately 1 week long baseline of the 2006 April light-curve data set we used $\dot{P} = (9.2 \pm 0.4) \times 10^{-11}$ s^{-1}. The pulsed fraction, the semiamplitude of modulation divided by the mean source count rate, is reported to the right of each panel.

advantage of a greater number of events (>40 between short bursts and IFs), therefore largely improving the statistics with which the detailed analysis can be carried out. The impact of the increased statistics and time resolution is evident when comparing the *Swift* results with previous ones. On 2001 July 2, the *HETE-2* instruments recorded a 3.5 s IF from SGR 1900+14, and a time-resolved ($\Delta t >$ 30 ms) spectral analysis was carried out in the 2–100 keV range (Olive et al. 2004). They found that the BB+BB model fitted the spectra well, the higher temperature BB evolving in a manner consistent with a shrinking emitting region and the lower temperature BB showing a constant radius. They also suggested that, within the magnetar model, the BB+BB model might be an approximation of a more complex multitemperature spectrum. Their Figures 5 and 7 can be easily compared with our Figures 4 and 5; the *Swift* data fill in those regions on the kT-R^2 plane which remained unexplored with *HETE-2*.

Several new properties can be immediately inferred. (1) The *Swift* data populate, almost homogeneously, all temperatures between ~2 and 12 keV, and the *HETE-2* measurements (Fig. 5, *black diamonds*) can be regarded as a subset of them. (2) The distribution is such that a sharp edge between the populated regions and the rest of the kT-R^2 plane is clearly present, with a cutoff (or sharp turn) in the distribution of $R_{\mathrm{BB}h}$ at $kT_h \approx 12$–13 keV. This sharp edge provides an estimate of the typical size of the relevant emitting regions (by assuming a reference distance of 10 kpc): 30–200 km for the BB_s component and 3–30 km for the BB_h component. (3) There is an additional turn in the BB_h component size between 6 and 16 km, at approximately 10 keV (see Fig. 5). (4) There is a strong correlation between kT and R^2_{BB} corresponding to the brightest phases of the IFs, which is consistent with a power law index of about −3 (while, if the luminosity were the same for all events, the relationship expected for a BB component would be $y = x^{-4}$, where $x = kT$ and $y = R^2_{\mathrm{BB}}$).

TABLE 5
THE TIMES OF SGR 1900+14 OUTBURSTS OCCURRING WHEN UVOT WAS TAKING DATA

Flare Time	Filter	Exp.	UL
2006 Mar 25, 23:34:07.748.....	UVM2 (2200 Å)	642	21.3
2006 Mar 26, 00:59:22.680.....	*V* (5460 Å)	213	18.9
2006 Mar 26, 13:30:04.620.....	*B* (4350 Å)	216	20.8
2006 Mar 26, 16:50:17.632.....	UVW2 (1930 Å)	851	20.9
2006 Mar 28, 20:32:31.456.....	UVM2 (2200 Å)	261	20.8
2006 Mar 29, 02:53:09.460.....	*V* (5460 Å)	1539	20.7

NOTE.—With the filter in use at the time (central wavelength in parentheses), exposure time of the image in seconds, and 3 σ magnitude upper limit at the XRT position.

The sharp edge in the distribution of the two-BB parameters suggests that a saturation effect occurs. In order to investigate this effect further, we divided the data points of the two BB components into two samples, below and above a bolometric luminosity of $L = 3 \times 10^{40}$ erg s^{-1} (see Fig. 5). The luminosity threshold was chosen so as to roughly separate the peaks of the bursts and flares from the interburst/flare time intervals. We note that the *HETE-2* data lie just above and below the flux threshold but never reach the values corresponding to the peaks and tops of the *Swift* IFs. As we can see from Figure 5, as long as each BB component is below $\sim 3 \times 10^{40}$ erg s^{-1}, their two luminosities are strongly correlated [$L(\mathrm{BB_{hard}})$ vs. $L(\mathrm{BB_{soft}})$ is well fitted by a power law index 0.7 ± 0.3 at 1 σ c.l.]. This correlation, which seems indicative of a physical link between the two BB components, was already noticed by Feroci et al. (2004), who analyzed the time-averaged spectral properties of 10 short bursts from SGR 1900+14 recorded by *BeppoSAX* in 2001 April (Fig. 6, *squares*). It is apparent that the *BeppoSAX* measurements are fully consistent with those obtained with *Swift* and can be regarded as a subsample of the latter. On the other hand, this trend was not reported by Olive et al. (2004) for the IF observed by *HETE-2* in 2001 (Fig. 6, *diamonds*). Intriguingly, the correlation no longer holds above $\sim 3 \times 10^{40}$ erg s^{-1} for the *Swift* data. Above this value, the luminosity of the BB_s component reaches a maximum in the $(7$–$14) \times 10^{40}$ erg s^{-1} range, while that of the BB_h component continues to increase up to $\sim 3 \times 10^{41}$ erg s^{-1}. Clearly, this previously unknown behavior strengthens the idea of a saturation mechanism in the burst emission.

The emission properties of the higher luminosity flares ($L > 3 \times 10^{40}$ erg s^{-1}) combined with the spectral information place some basic constraints on their production mechanism. The possible location of the emitting region and the main processes likely involved in shaping the spectra have been discussed by TD95. Lyubarsky (2002) studied the propagation of a trapped fireball through the ultramagnetized magnetosphere and computed an approximate emission spectrum for it. However, the comparison of these predictions with the results from our observations or those by Olive et al. (2004) is not straightforward. As already noted by Olive et al. (2004), the "modified blackbody" proposed by Lyubarsky (2002) predicts a significant depression below the

BB of the higher energy tail, which is not found in the data (the fit remains good up to energies of $\sim$100 keV). Clearly, more detailed spectral models for the burst are required.

In the following, we concentrate on important new information (mainly concerning the brightest part of IFs) which has been inferred from our spectral analysis. In particular, we discuss in detail three main findings: (1) the existence of two BB components, the harder one ($kT_h \sim 7$–11 keV) having a systematically smaller radius ($R_{\mathrm{BB}h} \leq 25$ km) than the softer one ($R_{\mathrm{BB}s} \sim 25$–100 km); (2) the existence of a clear correlation between the luminosities of the two components up to $\sim 3 \times 10^{40}$ erg s^{-1}, above which the luminosity of the softer BB shows signs of saturation, while that of the harder BB still grows up to a few times 10^{41} erg s^{-1}; and (3) the existence of a correlation between temperature and BB radius, which holds for the most luminous parts of the flares (approximately $L_{\mathrm{tot}} > 4 \times 10^{40}$ erg s^{-1}).

The first finding shows that different thermal components originate from different regions around the NS, ranging from its surface (at $R < R_{\mathrm{NS}}$) to well up in the magnetosphere, at a height of several stellar radii. The maximum observed flare luminosity is $\sim 3 \times 10^{41}$ erg s^{-1}, attained by the hard BB component at an effective temperature of $\sim$10 keV and radius of $\sim$15 km. Interestingly, this matches well with the magnetic Eddington luminosity, $L_{\mathrm{Edd},B}$, at that same radius, for a surface dipole field of $\simeq 8 \times 10^{14}$ G (this value of the B field is very close to that deduced from the spin-down rate of SGR 1900+14), where (Paczyński 1992; TD95)

$$L_{\mathrm{Edd},B}(r) \simeq 2 L_{\mathrm{Edd}} \left(\frac{B}{10^{12}\ \mathrm{G}} \right)^{4/3} \approx 2 \times 10^{40} \left(\frac{B}{B_{\mathrm{QED}}} \right)^{4/3} \left(\frac{r}{R_{\mathrm{NS}}} \right)^{2/3} \mathrm{erg\ s^{-1}}. \quad (1)$$

If radiation originated from a trapped hot fireball, this would be in line with the discussion of Thompson & Duncan (2001) and TD95, according to which the radiative efficiency of a magnetic confined fireball never exceeds (to within a small factor) the magnetic Eddington flux. In fact, ablation of matter from the NS surface would increase the scattering depth in a super-Eddington radiation field, thus providing a self-regulating mechanism. The radius and temperature that we inferred at maximum burst luminosity are also in good agreement with the prediction for the emission coming from a trapped fireball (TD95; see their discussion of the best-fit temperature and radius in the case of SGR 1806−20).

Most remarkably, we find that the luminosity of the soft component can be larger than 10^{40} erg s^{-1} out to $R \sim 100$ km. For $R_s > 30$–40 km this value exceeds the magnetic Eddington luminosity at the corresponding radius (for a dipole field geometry) and suggests that magnetospheric confinement plays an active role out to those distances, with magnetic stresses balancing radiation forces. If this were the case, the saturation of the soft component at $\simeq 10^{41}$ erg s^{-1} would be related to the magnetic field strength at the relevant radii and its maximum ability to retain the trapped fireball matter, which is subject to very high radiation pressure. A detailed investigation of the possible equilibrium configurations is beyond the scope of this paper and will be addressed in future work.

Our second finding (point 2) implies that, in the luminosity range 10^{40}–10^{41} erg s^{-1}, the total radiation energy is divided almost equally between the two components. Combining the information of Figures 5 and 6, we can see that, for a given luminosity $\leq 10^{41}$ erg s^{-1}, there are two separate emission regions: a smaller and hotter one, whose radiating area suggests emission from (part of) the NS surface with a relatively high effective temperature (10–12 keV), and a second, possibly magnetospheric region with a significantly larger emitting area and lower effective temperature (3–7 keV). The hotter component attains the highest luminosities, i.e., $>10^{41}$ erg s^{-1}, as its radius grows slightly and the effective temperature decreases. On the other hand, the colder component is characterized by a minimum BB radius of $\sim$25 km and maximum temperature of $\sim$7 keV.

A possible interpretation involves the different ways in which photons with ordinary (O) or extraordinary (E) polarization mode (a property introduced by the presence of a birefringent medium, such as the magnetic field; Mészáros et al. 1980) propagate across the magnetosphere. Since the scattering cross section of E-mode photons is much reduced in the presence of strong magnetic fields, E-mode photons have a scattering photosphere which is located much closer to the NS than that of O-mode photons. On the other hand, in a supercritical magnetic field ($B > B_{\mathrm{QED}}$), E-mode photons have a nonnegligible probability of splitting (and switching to the O mode). The probability is a strong function of energy, so that E-mode photons of high energy cannot travel far from their scattering photosphere before splitting into O-mode photons. On the other hand, O-mode photons will be entrained with streaming electrons and baryons and advected out to where their scattering optical depth becomes $\tau(O) \sim 1$ (TD95; Lyubarsky 2002). As a consequence of Compton scattering (and, with lower efficiency, photon merging), a fraction of O-mode photons can also switch back to the E mode. Therefore, the two modes are effectively coupled and are advected at comparable rates as long as mode switching is efficient; an approximately equal distribution of energy in the two modes is thus to be expected (TD95; Lyubarsky 2002). This may suggest that the two observed spectral components reflect the population of photons in the two polarization modes and, thus, the regions from which they are emitted.

We note that the minimum radius of the cold BB almost corresponds to the maximum radius of the hot component, the distribution of points in the R^2 versus kT plane being continuous across this point (see Fig. 5). This suggests the existence of a narrow zone of separation between the two emission regions. In order to further characterize this zone, we studied the R^2 versus kT distribution for each of the seven longest IFs and one short burst, which we discussed in previous sections (see also Table 3 and Fig. 11). Remarkably, the transition between the two BB components is more evident for the brightest flares (IF1 and IF7 in Fig. 11), where the upper left edge of the parameter distribution of the hard component is confined to smaller radii ($R \leq 20$ km) and correspondingly higher temperatures ($kT \geq 8$ keV). The soft component seems less dependent on the flux than the hard one, its minimum size being of the order of $\geq$25–35 km in all IFs. Qualitatively, this behavior is in agreement with the above scenario. In fact, a larger brightness can be reached when the burst energy is trapped closer to the NS surface, where the stronger magnetic field allows a larger flux (of E-mode photons) to be released. Moreover, the sharp and narrow gap between the emitting regions of the two BBs, at a radius of ($\sim$20–30 km), can be interpreted as the signature of the presence of an E-mode splitting photosphere (TD95); this represents the surface (at radius $R = R_{\mathrm{QED}}$) below which the magnetic field is supercritical ($B \geq B_{\mathrm{QED}}$), photon splitting is efficient, and the two polarization modes can remain coupled. E-mode photons can stream freely to the observer from the splitting photosphere (at radius $R_{\mathrm{QED}} \sim 20$–30 km), which then would naturally define a maximum size for the emission region of radiation in this polarization mode. On the other hand, O-mode photons

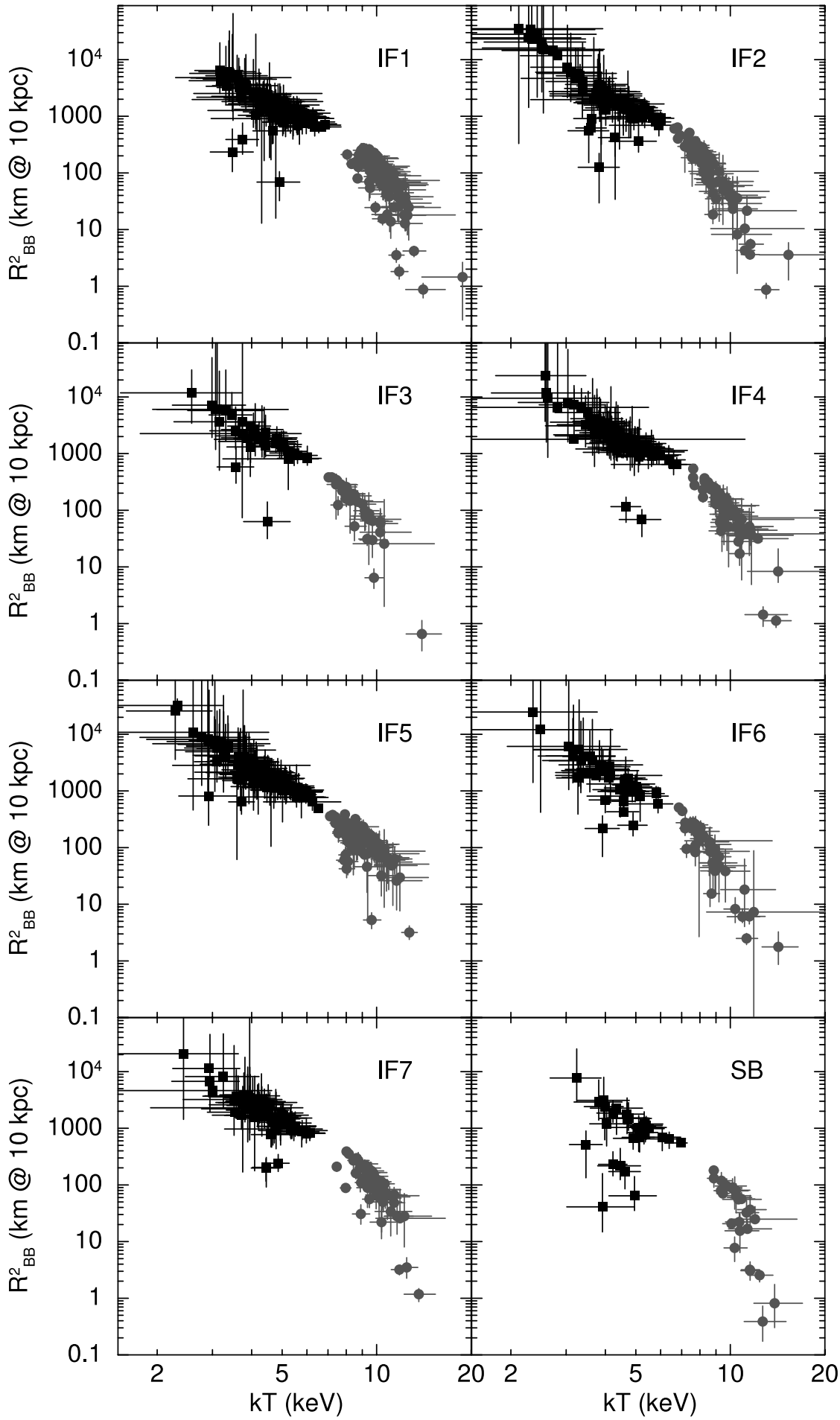

FIG. 11.—Same as Fig. 5, but for each of the seven longest IFs (IF1 to IF7) plus a short burst (SB) also reported in Table 3.

cannot originate from regions in the splitting photosphere, as their scattering optical depth is still much larger than unity within that volume.

If this scenario is correct, it implies that the emission region of E-mode photons can range from the base of the trapped fireball (near the NS surface) to a slightly higher region in the magnetosphere, but well within the splitting photosphere. In this case, part of the internal energy of the coupled E- and O-mode photons is lost in the E-mode photosphere (adiabatic) expansion from near the NS to the splitting photosphere. This degrades the original spectrum toward lower temperatures and larger radii, up to $R_{\rm QED}$. On the other hand, O-mode photons might be either released near the splitting photosphere or advected to much larger radii, depending on the value of their optical depth at that location (see TD95). In any case an improved treatment of the above effects would be required in order to develop a self-consistent model.

Finally, our third finding is the apparent correlation between the surface and temperature of the spectral components at different luminosities. This behavior does not have a clear interpretation. As shown in Figure 5, the top part of the data strip is well fit by a power law $\Sigma \propto T_{\rm BB}^{-3}$, where Σ is the radiating BB surface. Since $\Sigma T_{\rm BB}^4 = L$, this implies $T_{\rm BB} \propto L$. Therefore, along lines of constant luminosity, the radiating surface would scale like T^{-4}, i.e., steeper than the data points (on the edge of the allowed region in the kT vs. R^2 plane). The $\Sigma T^3 = {\rm const}$ relation implies a roughly constant number of emitted photons per unit time.

At the highest luminosities ($\geq 10^{41}$ erg s^{-1}) of the flares, where the softer BB saturates, the observed correlation involves both components. It is tempting to attribute this to the fact that, in this luminosity range, Comptonization and/or adiabatic losses play a dominant role in the formation of the emerging spectrum, both processes being characterized by conservation of the photon number (photon splitting should have only a minor impact). This is in agreement with the prediction by TD95 that, at effective temperatures less than $\sim$10 keV, photon splitting would not be efficient in maintaining a pure Planck spectrum for both modes. However, if the photon chemical potential is sufficiently small compared to the photon temperature, deviations from a Planck spectrum are expected only at low energies (TD95; Lyubarsky 2002), which we do not observe, given that they are masked by absorption.

On the other hand, at luminosities $\leq 10^{41}$ erg s^{-1}, the two BBs approximately share the same luminosity; therefore, the colder one emits a larger number of photons. This suggests that efficient photon number-changing processes (such as photon splitting or double Compton scattering) may play a key role in the formation of the spectrum. Indeed, we note that the photon number ratio is roughly the same as the temperature ratio in this case, since the luminosities are approximately equal. As this ratio peaks around 2 and extends from 1.5 and 4, it appears to be qualitatively compatible with the combined effects of photon splitting and double Compton scattering (Lyubarsky 2002).

Finally, we briefly comment on the sharp turn in the hard component distribution at around $kT \sim 10$ keV and subsequent cutoff at $\sim$12/14 keV, which, together with the $\Sigma T^3 = {\rm const}$ relation, are among the most distinctive properties of Figure 5. Among others, these features clearly imply that no thermal component with a characteristic temperature above the cutoff is detected, although the BAT energy interval extends up to at least 100 keV. Within the discussed scenario it is tempting to account for the above properties in terms of the photon-splitting process and, in particular, its efficiency as a function of (mainly) flux and energy. In fact, the turn at $kT \sim 10$ keV marks the drift of the parameter distribution from the $\Sigma T^3 = {\rm const}$ relation, identifying the passage between photon number conservation (such as Comptonization) and photon number changing (photon-splitting) emitting processes. As reported by TD95, the minimum temperature at which photon splitting is efficient in maintaining a nearly Planckian spectrum for E-mode photons is $\simeq$10 keV.

3.2. *The Persistent Emission*

The *Swift* XRT monitoring data allowed us to study the evolution of the persistent emission of SGR 1900+14 on relatively short timescales, starting from 1 day before up to one and a half months after the BAT event. We clearly detected a spectral evolution in the higher energy end of the 1–10 keV spectrum as a function of flux. The PL component becomes flatter for larger fluxes. The changes in the persistent component are temporary and last for approximately a couple of weeks, while we detect variability on daily timescales. It is also interesting to note that the spectral results we obtained on 2006 April 8 (see P3 interval in Table 4, the green lines in Fig. 7, and the gray lines in Figs. 8 and 9) are consistent, to within the uncertainties, with those reported by Mereghetti et al. (2006) from a deeper Target-of-Opportunity *XMM-Newton* observation carried out on 2006 March 1.

Both AXPs and SGRs have shown a correlation between the X-ray flux and the spectral hardness (see, e.g., Woods et al. 2007; Rea et al. 2005a); this has been explained in terms of the onset of a "twist" in the magnetosphere. As discussed by Thompson et al. (2002), a magnetar may differ from standard radio pulsars because its magnetic field is globally twisted inside the star, up to a strength of about 10 times the external dipole, and occasionally this field is expected to fracture the crust and lead to a twist of the external field. The basic idea is that when such a twist is formed, currents flow into the magnetosphere. As the twist angle $\Delta\phi_{\rm NS}$ grows, electrons provide an increasing optical depth to resonant cyclotron scattering, leading to the buildup of a flatter photon power-law component. At the same time, larger returning currents produce extra heating of the star surface and increased X-ray flux. Therefore, both increased activity and glitches are expected to be associated with erratic fracturing of the crust. Observations obtained until 2003 were consistent with a scenario in which the twist angle was steadily increasing before the glitch epochs, culminating in glitch(es) and periods of increased timing noise, and then decreasing, leading to a smaller flux and a softer spectrum. The decay time of the global twist is given by (Thompson et al. 2002)

$$t_{\rm decay} \simeq 40 \Delta\phi_{\rm N\text{-}S}^2 \left(\frac{L_{\rm X}}{10^{35}\ {\rm erg\ s^{-1}}}\right)^{-1} \left(\frac{B_{\rm pole}}{10^{14}\ {\rm G}}\right)^{2} \left(\frac{R_{\rm NS}}{10\ {\rm km}}\right)^{3} {\rm yr}, \quad (2)$$

where $\Delta\phi_{\rm N\text{-}S}$ is the net twist between the north and south magnetic hemispheres and $B_{\rm pole}$ is the magnetic field strength at the pole(s). By using the inferred persistent unabsorbed luminosity of SGR 1900+14 ($\sim 10^{35}$ erg s^{-1}) and the observed time interval (of the order of $<$1 month) over which the spectral parameters change and return to the preburst forest event, and assuming a standard size for the NS surface and 10^{14} G $< B_{\rm pole} < 10^{15}$ G, we infer a twist angle in the few $\times\ 10^{-3}$ to few $\times\ 10^{-2}$ rad interval, which is similar to that inferred for the bursting AXP 1E 2259+586 ($\sim 10^{-2}$ rad; Woods et al. 2004).

We regard it as unlikely that the hardening and softening of the power-law component (in the 1–10 keV band) is due to a change in the flux and/or photon index of the additional power-law component detected by *INTEGRAL* in the 20–200 keV band flux of several AXPs and SGRs (Kuiper et al. 2006; the SGR 1900+14

emission above 20 keV was also rediscovered by the PDS on board *BeppoSAX*; Götz et al. 2006; Esposito et al. 2007). This is implied by the finding that the spectrum of SGR 1900+14 can be accounted for by only one power-law component covering both the soft and hard X-rays (from ~1 to ~200 keV).

We monitored the pulse shape and pulse fraction of the ~5.2 s spin period modulation through a timing analysis of the persistent component. Large changes were detected as a function of flux (see Fig. 10); pulses appear to be less pulsed but more structured (to within the uncertainties) and with smaller relative amplitude for increasing fluxes. Such a flux dependence of the pulse properties was already detected in other SGRs and AXPs and related to changes in the persistent emission component. Among SGRs, SGR 1806−20 showed a decrease in the pulsed fraction together with the appearance of additional peaks in the pulse profile after the giant flare of 2004 December 27 (Rea et al. 2005b; Woods et al. 2007). More recently, similar behavior was observed in the transient AXP CXOU J164710.2−455216 in correspondence to the onset of an outburst (Israel et al. 2007a). Given the almost constant properties of the BB component, variations are likely due to the PL component, which is supposed to originate in the magnetosphere. In particular, the pulse shape changes may indicate an evolution of the geometry of the magnetosphere. Alternatively, the magnetosphere may randomize the outcoming pulsed photons, temporarily decreasing the pulsed fraction.

4. CONCLUSIONS

On 2006 March 29, after several days of burst activity, the soft gamma-ray repeater SGR 1900+14 displayed a series of short bursts and intermediate flares (IFs) lasting for about 30 s, during which all the *Swift* instruments were pointed to the source. The good statistics, the fine time resolution (4 ms), and the wide energy coverage (0.2–100 keV) allowed us to carry out a detailed study of the timing and spectral properties during both the bursts and the persistent emission. Large variations were detected and their evolution studied over a range of timescales. Although not all the observational properties can be accounted for by the current magnetar scenario, the large majority of them are in overall good agreement with it. In particular, we found the following:

1. A break around $\sim 10^{41}$ erg s^{-1} in the known correlation between the luminosities of the two blackbody components which well fit the BAT time-resolved and BAT+XRT integrated spectra. Above this value the softer blackbody shows signs of saturation, while the luminosity of the harder blackbody still increases up to $\sim 3 \times 10^{41}$ erg s^{-1}.
2. The existence of a correlation between temperature and emitting surface of the blackbodies ($R^2 \propto kT^{-3}$), which holds through the most luminous phases of the flares ($L_{\rm tot} \geq 10^{41}$ erg s^{-1}).

The above two findings together can be interpreted in terms of the two populations of photons from the O- and E-mode polarizations, which are foreseen in the magnetar scenario, and the regions from which they escape: the larger and colder the O-mode photon region, the harder and smaller the E-mode region.

Moreover, we note that the maximum observed luminosity from flares ($\sim 3 \times 10^{41}$ erg s^{-1}) is attained by the harder blackbody component at an effective temperature of ~10 keV and radius of ~15 km, which is similar to the inferred magnetic Eddington luminosity at the same radius, for a surface dipole field of $\simeq 8 \times 10^{14}$ G (as deduced from the spin-down of SGR 1900+14).

Finally, based on our analysis, we do not see any significant difference between IFs and short bursts. Both IFs and short bursts seem to form a continuum in terms of spectral properties (besides duration and fluence).

As far as the persistent emission properties are concerned, we found the following:

1. A clear correlation between the PL photon index Γ and the persistent flux, such that flatter PL components correspond to larger fluxes. The source returned to the usual spectral shape approximately 1 week after the burst "forest" event.
2. Changes in the modulation of the 5.2 s spin period, with the pulse profiles becoming more structured (to within the uncertainties) for increasing persistent flux. The pulse properties returned to their usual state within 1 week as well.

The above results are not dissimilar from those observed in other magnetar candidates, although this is the first time that variations have been detected on timescales of 1 hr (for the pulses) and days (for the spectra). These findings are qualitatively in agreement with the expected properties of a "twisted" magnetosphere.

More generally, the unprecedented high quality of the *Swift* data allowed us to gather important new insights into the emission mechanism properties at a detail level which had not been attained before. We hope that findings like the ones presented in this paper will stimulate a more detailed theoretical treatment of the physics of SGR and AXP bursts.

This work is partially supported at OAR through Agenzia Spaziale Italiana (ASI), Ministero dell'Istruzione, Università e Ricerca Scientifica e Tecnologica (MIUR-COFIN), and Istituto Nazionale di Astrofisica (INAF) grants. This work is supported at OAB and OAR by ASI grants I/011/07/0 and I/088/06/0 and at OAB by MIUR PRIN 2005025417. We gratefully acknowledge the contributions of dozens of members of the BAT, XRT, and UVOT Teams at OAB, PSU, UL, GSFC, ASDC, and MSSL and their subcontractors, who helped make the *Swift* mission possible. G. L. I. would like to thank Alaa Ibrahim for useful discussions on the comparison between the burst spectral properties of SGR 1806−20 and SGR 1900+14, Marco Feroci for comparison with burst properties of SGR 1900+14 as observed by *BeppoSAX*, and Peter Woods for careful reading of the manuscript and valuable suggestions for its improvement.

Facilities: Swift (XRT), Swift (BAT), Swift (UVOT)

REFERENCES

Akerlof, C., et al. 2000, ApJ, 542, 251
Anders, E., & Grevesse, N. 1989, Geochim. Cosmochim. Acta, 53, 197
Aptekar, R. L., Frederiks, D. D., Golenetskii, S. V., Il'inskii, V. N., Mazets, E. P., Pal'shin, V. D., Butterworth, P. S., & Cline, T. L. 2001, ApJS, 137, 227
Barthelmy, S. D., et al. 2005, Space Sci. Rev., 120, 143
Burrows, D. N., et al. 2005, Space Sci. Rev., 120, 165
Duncan, R. C., & Thompson, C. 1992, ApJ, 392, L9
Eikenberry, S. S., Garske, M. A., Hu, D., Jackson, M. A., Patel, S. G., Barry, D. J., Colonno, M. R., & Houck, J. R. 2001, ApJ, 563, L133
Esposito, P., Mereghetti, S., Tiengo, A., Sidoli, L., Feroci, M., & Woods, P. 2007, A&A, 461, 605
Fenimore, E. E., Laros, J. G., & Ulmer, A. 1994, ApJ, 432, 742
Feroci, M., Caliandro, G. A., Massaro, E., Mereghetti, S., & Woods, P. M. 2004, ApJ, 612, 408
Fuchs, Y., Mirabel, F., Chaty, S., Claret, A., Cesarsky, C. J., & Cesarsky, D. A. 1999, A&A, 350, 891
Götz, D., Mereghetti, S., Tiengo, A., & Esposito, P. 2006, A&A, 449, L31
Guidorzi, C., Frontera, F., Montanari, E., Feroci, M., Amati, L., Costa, E., & Orlandini, M. 2004, A&A, 416, 297
Hill, J. E., et al. 2004, Proc. SPIE, 5165, 217
Hurley, K., Kouveliotou, C., Woods, P., Cline, T., Butterworth, P., Mazets, E., Golenetskii, S., & Frederics, D. 1999, ApJ, 510, L107
Israel, G. L., Campana, S., Dall'Osso, S., Muno, M. P., Cummings, J., Perna, R., & Stella, L. 2007a, ApJ, 664, 448

Israel, G. L., Götz, D., Zane, S., Dall'Osso, S., Rea, N., & Stella, L. 2007b, A&A, 476, L9
Israel, G. L., et al. 2005, ApJ, 628, L53
Kouveliotou, C., et al. 1993, Nature, 362, 728
———. 1998, Nature, 393, 235
———. 1999, ApJ, 510, L115
———. 2001, ApJ, 558, L47
Kuiper, L., Hermsen, W., den Hartog, P. R., & Collmar, W. 2006, ApJ, 645, 556
Laros, J. G., Fenimore, E. E., Fikani, M. M., Klebesadel, R. W., & Barat, C. 1986, Nature, 322, 152
Lodders, K. 2003, ApJ, 591, 1220
Lyubarsky, Y. E. 2002, MNRAS, 332, 199
Mazets, E. P., Cline, T. L., Aptekar, R. L., Butterworth, P. S., Frederiks, D. D., Golenetskii, S. V., Il'Inskii, V. N., & Pal'Shin, V. D. 1999, Astron. Lett., 25, 628
Mazets, E. P., & Golenetskii, S. V. 1981, Ap&SS, 75, 47
Mereghetti, S., et al. 2005, ApJ, 628, 938
———. 2006, ApJ, 653, 1423
Mészáros, P., Nagel, W., & Ventura, J. 1980, ApJ, 238, 1066
Nakagawa, Y. E., et al. 2007, PASJ, 59, 653
Olive, J.-F., et al. 2004, ApJ, 616, 1148
Paczyński, B. 1992, Acta Astron., 42, 145
Palmer, D. M., Sakamoto, T., Barthelmy, S., Cummings, J., Gehrels, N., Krimm, H., Markwardt, C., & Tueller, J. 2006, ATel, 789, 1
Rea, N., Oosterbroek, T., Zane, S., Turolla, R., Méndez, M., Israel, G. L., Stella, L., & Haberl, F. 2005a, MNRAS, 361, 710
Rea, N., Tiengo, A., Mereghetti, S., Israel, G. L., Zane, S., Turolla, R., & Stella, L. 2005b, ApJ, 627, L133
Romano, P., Barthelmy, S. D., Kennea, J. A., Markwardt, C. B., Moretti, A., & Palmer, D. M. 2006a, GCN Circ. 4934, http://gcn.gsfc.nasa.gov/gcn3/4934.gcn3
Romano, P., et al. 2006b, A&A, 456, 917
Roming, P. W. A., et al. 2005, Space Sci. Rev., 120, 95
Schwartz, S. J., et al. 2005, ApJ, 627, L129
Strohmayer, T. E., & Ibrahim, A. I. 2000, ApJ, 537, L111
Strohmayer, T. E., & Watts, A. L. 2005, ApJ, 632, L111
Thompson, C., & Duncan, R. C. 1995, MNRAS, 275, 255 (TD95)
———. 1996, ApJ, 473, 322
———. 2001, ApJ, 561, 980
Thompson, C., Lyutikov, M., & Kulkarni, S. R. 2002, ApJ, 574, 332
Titarchuk, L. 1994, ApJ, 434, 570
Vrba, F. J., Henden, A. A., Luginbuhl, C. B., Guetter, H. H., Hartmann, D. H., & Klose, S. 2000, ApJ, 533, L17
Woods, P. M., Kouveliotou, C., Finger, M. H., Göğüş, E., Wilson, C. A., Patel, S. K., Hurley, K., & Swank, J. H. 2007, ApJ, 654, 470
Woods, P. M., Kouveliotou, C., van Paradijs, J., Finger, M. H., & Thompson, C. 1999, ApJ, 518, L103
Woods, P. M., & Thompson, C. 2006, in Compact Stellar X-ray Sources, ed. W. Lewin & M. van der Klis (Cambridge: Cambridge Univ. Press), 547
Woods, P. M., et al. 2004, ApJ, 605, 378